Knowledge-Informed Wheel Wear Prediction Method for High-Speed Train Using Multisource Signal Data

Chen Chen, *Student Member, IEEE*, Feng Zhu, Zhongwei Xu, Qinglin Xie, *Graduate Student Member, IEEE*, Siu Ming Lo, Kwok Leung Tsui, and Lishuai Li, *Senior Member, IEEE*

***Abstract*— Wear prediction for train wheels is essential for evaluating the health status of wheel-rail systems. Existing prediction approaches mainly focus on the physics-based approach or data-driven approach, which either involve complex mechanisms or lack interpretability. A data-driven wear prediction method regarding domain knowledge and multisource signals is developed herein to improve the difficulties in the two approaches. The presented method involves three modules. First, axle box acceleration (ABA) data are investigated via spectral analysis, and domain knowledge associated with wheel wear degradation is concluded. Then, data fusion and feature extraction are performed to modify the vertical ABA signals and extract effective features. Next, a supervised regression model is built to predict wheel tread wear using the extracted feature and wear data. While the model is established, on-board monitoring for wheel tread wear can be realized by inputting the measured ABA signals. The performance of our method is evaluated and tested on real-world data from three service lines. Experimental results show that the developed method performs satisfactorily in terms of mean absolute percentage error, root mean square error, and R^2, registering average values of 0.0939, 0.0224, and 0.9457, respectively.**

***Index Terms*— Health monitoring, high-speed rail (HSR), support vector regression (SVR), vibration data, wheel tread wear.**

I. Introduction

CHINA'S high-speed rail (HSR) networks had extended over an impressive 45 000 km by the end of 2023, representing approximately two-thirds of global HSR networks [1]. As HSR systems have become a crucial aspect of transportation infrastructure across multiple continents, their safety and reliability are increasingly prioritized. Wheels are essential components of high-speed trains for carrying, guiding, and braking. However, the operation of high-speed trains inevitably causes wheel wear. This degradation not only directly affects operational safety and ride comfort, which are two paramount concerns for railway agencies, but also can lead to more severe consequences if not properly managed. Thus, routine monitoring of the wheel wear status has become a focal point in the operations and maintenance (O&M) activities of HSR systems [2].

Current practices for monitoring and maintaining wheel wear predominantly rely on tracking the operating mileage and conducting regular wheel profile measurements. These methods significantly increase the workload and consequent costs associated with routine O&M activities [3], [4]. However, with the advent of prognostics and health management (PHM) approaches, there has been a shift toward developing innovative applications to predict wheel wear based on-board sensors. Such approaches can significantly reduce the O&M costs of HSR systems.

Most current research on predicting wheel wear on high-speed trains is based on physical models. These models incorporate vehicle dynamics theories, wheel-rail contact, and wheel-track material interaction to predict wheel wear. To construct accurate wheel-wear prediction models, detailed investigations [5], [6], [7], [8] have been conducted into the dynamic characteristics of high-speed trains and the wheel-rail contact theory. By leveraging the knowledge gained from these investigations, various wheel wear prediction models have been proposed. For example, Zobory [9], along with Szabó and Zobory [10], employed Hertzian contact theory and the FASTSIM algorithm to calculate the wheel-rail contact force. The dynamic response was analyzed using the ELDACW software, and a wear model was established to predict the wheel wear. Archard [11] postulated a correlation among the extent of wear, material properties, and relative sliding distance, leading to the formulation of Archard's material wear model. The uncertainty inherent in the Archard model was further analyzed by da Silva and Pintaude [12]. Li et al. [13] combined vehicle dynamics with Archard's model to simulate the tread wear in high-speed trains. Although existing studies affirm the effectiveness of physics-based methods for predicting wheel

Manuscript received 8 March 2024; accepted 19 May 2024. Date of publication 12 June 2024; date of current version 24 June 2024. This work was supported in part by the National Key Research and Development Program of China under Grant 2022YFB4300504-4 and in part by the Hong Kong Research Grants Council (RGC) Research Impact Fund under Grant R5020-18. The Associate Editor coordinating the review process was Dr. Dan Zhang. *(Corresponding author: Lishuai Li.)*

Chen Chen is with the School of Electronics and Information Engineering, Tongji University, Shanghai 201804, China, and also with the School of Data Science, City University of Hong Kong, Kowloon, Hong Kong (e-mail: cchen386-c@my.cityu.edu.hk).

Feng Zhu and Siu Ming Lo are with the College of Engineering, City University of Hong Kong, Kowloon, Hong Kong (e-mail: fenzhu2-c@my.cityu.edu.hk; sm.lo@cityu.edu.hk).

Zhongwei Xu is with the School of Electronics and Information Engineering, Tongji University, Shanghai 201804, China (e-mail: xuzhongweish@163.com).

Qinglin Xie is with the State Key Laboratory of Traction Power, Southwest Jiaotong University, Chengdu 610031, China (e-mail: qlxie@my.swjtu.edu.cn).

Kwok Leung Tsui is with the Grado Department of Industrial and Systems Engineering, Virginia Polytechnic Institute and State University, Blacksburg, VA 24061 USA (e-mail: kltsui@vt.edu).

Lishuai Li is with the School of Data Science, City University of Hong Kong, Kowloon, Hong Kong (e-mail: lishuai.li@cityu.edu.hk).

Digital Object Identifier 10.1109/TIM.2024.3413151

wear, these approaches may lack broad applicability because of the complex and unpredictable nature of train operational statuses. Additionally, the procurement of all necessary parameters for the modeling process is challenging, further inhibiting the comprehensive application of these methods.

The accumulation of on-board data and advancements in data analytics enable the development of data-driven wheel-wear prediction models. For example, Huang et al. [14] constructed effective features from temperature data using principal component analysis and the wrapper method. These features were considered to train a nonlinear autoregressive model to predict the wheel tread wear. Han and Zhang [15] analyzed the statistical characteristics of wheel wear and proposed a binary wheel-wear prediction model. Xu et al. [16] conducted a time–frequency analysis of train vibration data and selected spectral energy as the feature to build a wear-prediction model. Deep learning (DL) has become popular for its powerful representation capabilities and is widely applied in HSR system condition monitoring. Chen et al. [17] developed a fault diagnosis algorithm based on a capsule network for a high-speed train bogie. Huang et al. [18] combined complete ensemble empirical mode decomposition with adaptive noise and a 1D-convolutional neural network for condition monitoring of train bogies. Wang et al. [19] proposed a novel transformer-based framework with multiplex local–global temporal fusion that can be used for wheel-wear prediction based on the collected vibration signals. Apparently, modeling approaches, whether based on traditional statistical machine learning (ML) or DL algorithms, significantly hinge on feature selection, which sets the upper limit of the model capabilities. Traditional statistical ML-based models, though widely used, exhibit limitations in feature learning ability and struggle to extract key features from the copious operational data available. In contrast, DL-based models boast superior automatic feature learning capabilities, often leading to enhanced model performance. However, both traditional statistical ML and DL approaches share a common drawback: they yield results that are less interpretable than those obtained from physics-based models. While these models can compute indicators of the system health status, they struggle to provide detailed health information, such as physical degradation parameters. Despite DL algorithms identifying key wheel wear features, their limited interpretability constrains utility. These restrictions manifest as trust issues, model complexity, generalization assessment challenges, and optimization difficulties. Such limitations affect the broad adoption and effective application of DL-based approaches in practice.

To bridge the gap between the physics-based and data-driven approaches, integrating domain knowledge is essential during the feature design and extraction stages. This approach proves particularly valuable when analyzing vibration signals obtained from various components such as bearings, gearboxes, and suspension systems. By employing spectral analysis and examining dynamic characteristics, it becomes feasible to extract critical, highly interpretable features for wheel wear prediction models. Building on the work of Zhai et al. [20], this study presents a knowledge-informed data-driven wheel-wear prediction method using multisource signal data. First, we delved deeper into the high-speed train's vibration characteristics and long-term performance, drawing further domain knowledge. Based on these insights, we designed a Kalman filter-based algorithm for extracting high-quality features for subsequent modeling. Finally, the effectiveness of the proposed method is verified by real-world datasets.

The primary advantages of the proposed method, relative to the existing method, are outlined as follows. First, the domain-knowledge-informed approach has bolstered the model's reliability and interpretability, enabling it to be trusted and more adaptable to real-world applications. Second, the proposed interpretable feature engineering is straightforward to implement, ensuring robust adaptability across different wheel systems. Interpretability can refine the model's focus, leading to more relevant feature selection and data representation, thus improving prediction accuracy. Third, the designed domain knowledge guide noise reduction method that augments the model's resistance to interference, allowing it to achieve satisfactory results even in the presence of high-intensity noise.

The remainder of this article is organized as follows. Section II describes the signal acquisition and wheel wear measurement details. The proposed method for prediction modeling is described in Section III. In Section IV, experiments and evaluation of the proposed method are presented. Finally, Section V provides the conclusion and proposes a potential direction for future research.

II. Operational Data Description

The real-world operational data considered in this study were gathered from a CRH1A-type train operating in China between August 2015 and June 2016. The State Key Laboratory of Traction Power's Test and Control Group at Southwest Jiaotong University continuously tracked train performance over ten months across three lines: Changsha–Huaihua (CH) line, Guangzhou–Zhuhai (GZ) line, and Sanya–Haikou (SH) line. Thirty trips were recorded, comprising 11 trips on the CH lines, 3 on the GZ line, and 16 on the SH loop line. The collected data include multilocation vibration acceleration, speed, and wheel wear data.

A. Multilocation Vibration Data and Speed Data

The vibration signals were measured using 11 on-board accelerometers, located as shown in Fig. 1, at three levels: the car body, bogie frame, and axle box. Vibration data from each accelerometer were captured in three orthogonal directions: vertical, lateral, and longitudinal. Consequently, 33 records were collected regarding each train's operation. The sensor information is listed in Table I. In this study, axle box acceleration (ABA) data were utilized to analyze the vibration behavior, determine the domain knowledge associated with wheel wear degradation, and build a wear prediction model. Speed data for the train were collected using a global positioning system (GPS). An example of the ABA data in three directions and the corresponding speed signal in one trip are depicted in Fig. 2. The group collected test data for speeds of 250 and 200 km/h. On the CH line, the trains operated at

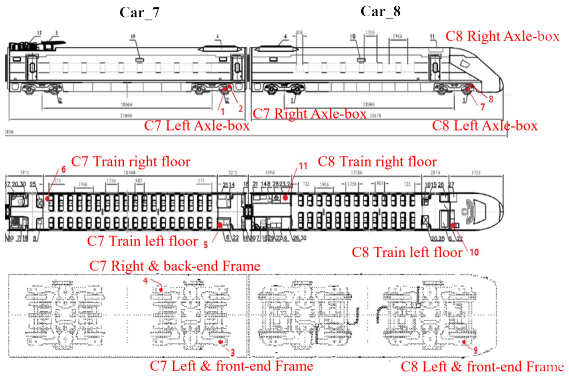

Fig. 1. Position of 11 vibration sensors on two cars. Car 7 (C7) is the trail car, and Car 8 (C8) is the motor car.

TABLE I
SENSOR INFORMATION FOR C7 AND C8

Number	Sensor position	Sampling frequency (Hz)	Type
1	Left axle box	5000	C 7
2	Right axle box		
3	Left frame	2000	
4	Right frame		
5	Left floor		
6	Right floor		
7	Left axle box	5000	C 8
8	Right axle box		
9	Left frame	2000	
10	Left floor		
11	Right floor		

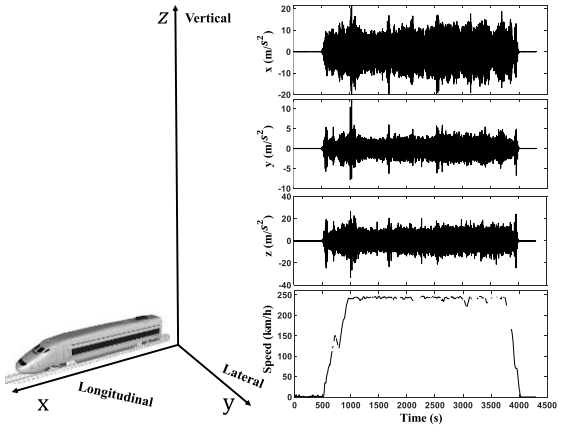

Fig. 2. Example of vibration signals from three directions and speed signal in one trip.

the speed of 250 km/h, while on the GZ and SH lines, the operational speed was maintained at 200 km/h.

B. Wheel Wear Data

The wheel profile was captured by Optimess Wheel Profile Sensor, and wear data were calculated accordingly. Fig. 3 shows the process of profile measurement and tread wear calculation. Within the coordinate diagram, the solid line delineates the original wheel profile, whereas the dashed line

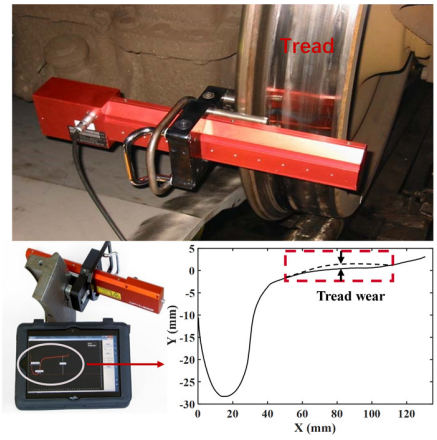

Fig. 3. Example of profile measurement and tread wear calculation.

represents the profile following tread wear. Data were collected regarding wheel treads and flange wear. In this study, the research object is wheel tread wear. According to the Railway Group Standard [21], [22], wheel tread wear refers to the wear of the wheel at the nominal rolling circle, which is calculated by comparing the profile curve between the measured and original baseline values in the wheel tread. By definition, the radially measured tread wear exhibits a significant physical correlation with the wheel radius.

III. METHODOLOGY

In this study, a data-driven framework is proposed for modeling and predicting wheel tread wear. The framework inputs are on-board ABA signals. The outputs are the tread wear of the train wheels. As shown in Fig. 4, there are three modules in the integral framework: 1) spectrum analysis and knowledge conclusion; 2) data fusion and feature extraction; and 3) regression modeling. A detailed description of this process is presented in Sections III-A–III-C.

A. Spectrum Analysis and Knowledge Conclusion

This section presents spectral analysis and the mechanism-based domain knowledge conclusion. The vibrational behavior is analyzed both in the frequency and time–frequency domains. Fourier-based data-processing methods are employed to process the original vibration data. Specifically, the fast Fourier transform (FFT) [23] is utilized for frequency-domain conversion. The short-time Fourier transform (STFT) [24] is adopted for time–frequency domain transformations. STFT is adept at processing nonstationary data and time-varying systems using a window function [25]. To diminish the amplitude skewness and discern the dominant frequency more distinctly in the time–frequency domain, a nonlinear normalization using log10 is executed [26], [27].

Zhai et al. [20] investigated the vertical and lateral vibrational behavior of a CRH train traveling at 350 km/h and identified the dominant frequency of the train components. This study adopts the same analytical approach and further investigates the vibrational behaviors in the longitudinal direction. Fig. 5 depicts the vibrational behavior of ABA

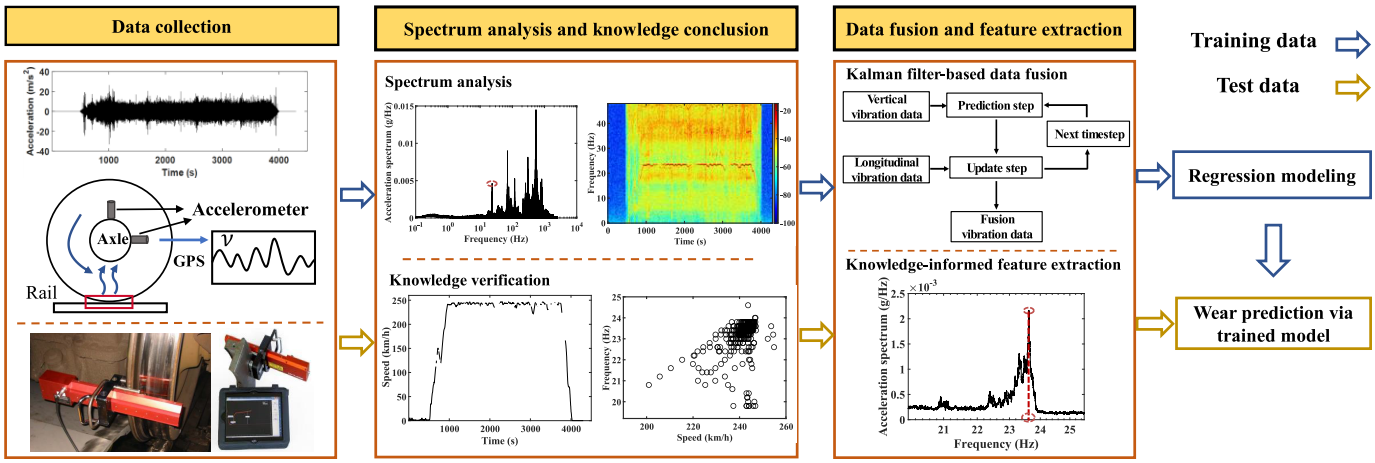

Fig. 4. Integral framework for wheel tread wear prediction.

in the vertical, longitudinal, and lateral directions within the frequency domain based on data from one trip on the CH line. The vibration performance is consistent with that reported by Zhai et al. [20]. As illustrated in Fig. 5(a), the vibrational characteristics of the vertical ABA predominantly manifest within two specific frequency ranges. The 10–100 Hz range represents the vibrations induced by the elasticity of the bogie frame and the wheel perimeter. Conversely, the 450–600 Hz range is associated with vibrations stemming from the elasticity in the Hertzian contact between the wheel and rail. Fig. 5(c) illustrates the vibrational behavior of the lateral ABA. Although it shares a similar vibration performance with the vertical ABA, a distinct dominant frequency emerges within the 20–30 Hz range, which is attributable to the vibrations stemming from the wheel perimeter. Fig. 5(b) shows the vibration performance of the longitudinal ABA. A distinct dominant frequency in the range of 20–30 Hz associated with the vibrations caused by the wheel perimeter also exists and demonstrates reduced noise compared with lateral vibrations. The vibration performance of the longitudinal ABA is consistent with that in the literature. Li et al. [28] determined that longitudinal ABA exhibits less noise than vertical and lateral ABAs.

This study focuses on the degradation process of wheel tread wear. Considering that wheel tread wear is derived from radial calculations [26], [27], it is strongly correlated with the wheel's radius or perimeter. The dominant frequency induced by wheel perimeter inspires us to explore its relationship with wheel tread wear. A pervasive challenge in our research and other HSR health-monitoring studies is the scarcity of data for direct analysis. The available vibration and wheel tread wear data in this study are notably limited, which limits the direct correlation analysis between the dominant frequency and wheel tread wear. Consequently, time-domain information is incorporated using STFT to delve into domain knowledge and investigate the correlation between the dominant frequency and wheel tread wear. Fig. 6 illustrates the ABA from the trip across three directions in the time–frequency domain. In Fig. 6(a), the spectrogram for the vertical ABA shows a dense and uniform distribution of energy across the time–frequency spectrum, which could indicate a high level of background noise masking the dominant frequency band. Conversely, Fig. 6(b), representing the longitudinal direction, exhibits a distinct and isolated frequency band, suggesting a clearer signal with less noise interference. Moreover, this dominant frequency band corresponds to speed fluctuations, exhibiting a consistent trend. The same dominant frequency band, with more noise, exists in the lateral ABA data, as shown in Fig. 6(c).

We used the region maximum function to extract longitudinal ABA's dominant frequency and speed vectors for correlation analysis. Fig. 7 presents a scatter plot illustrating the positive correlations between the two variables. Additionally, Pearson's correlation coefficient is used to assess the correlation between them. The calculated Pearson correlation coefficient is 0.9, indicating a strong linear correlation. Considering these physical phenomena, the dominant frequency–speed relationship can be represented by

$$f_z = k \cdot v \tag{1}$$

where f_z denotes the dominant frequency induced by the wheel perimeter. k denotes the proportional coefficient and v denotes the speed of the train. It is worth mentioning that (1) lacks a constant term because, in this context, the dominant frequency directly stems from the wheel's rotation over the rail, theoretically equating to zero at a standstill train speed.

As the wheel rotates, the relationship between angular velocity v and radius R can be expressed as

$$f_\omega = \frac{v}{2\pi R} \tag{2}$$

where f_ω is the wheel rolling frequency and R is the wheel radius.

As previously described, the wheel tread wear is closely associated with the wheel radius. Our objective is to investigate the correlation between f_z and R, which would subsequently illuminate the relationship between f_z and wheel tread wear. Inspired by the (1) and (2), we postulate that $f_z = f_\omega$. Consequently, the relationship between f_z and R can be

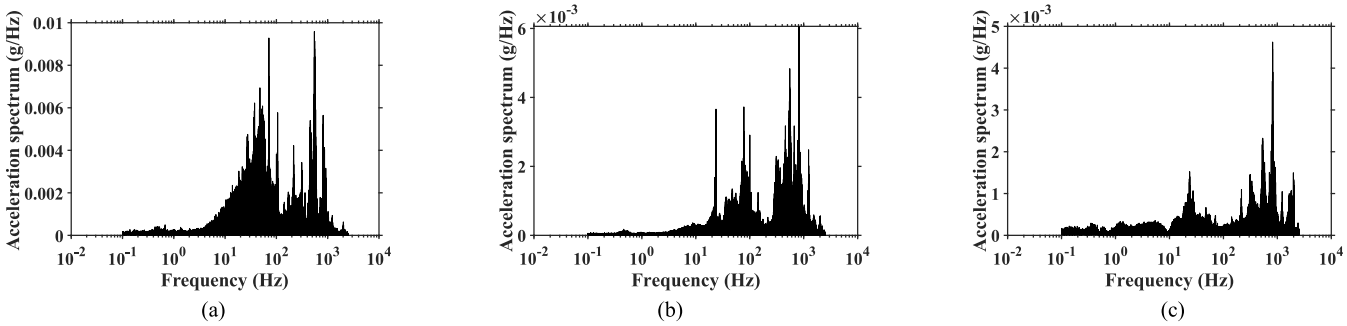

Fig. 5. ABA data of one trip from three directions in the frequency domain. (a) Vertical direction. (b) Longitudinal direction. (c) Lateral direction.

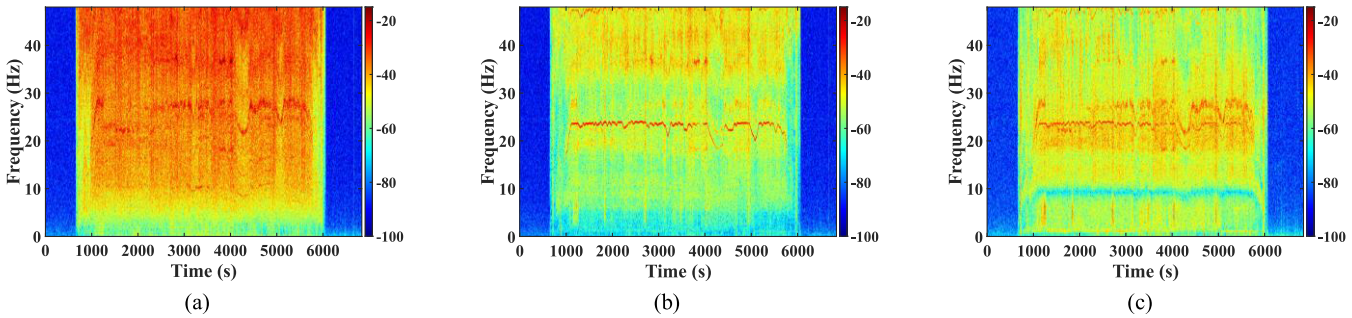

Fig. 6. ABA data of one trip from three directions in the time–frequency domain. (a) Vertical direction. (b) Longitudinal direction. (c) Lateral direction.

Fig. 7. Analysis of the correlation between the dominant frequency and speed signal.

denoted by the following equation:

$$f_z = f_\omega = \frac{v}{2\pi R}. \tag{3}$$

With the relationship in (3), f_z has a strong physical meaning for wheel tread wear. To prove (3), the following auxiliary proof is introduced. First-order eccentric wear is prevalent in HSR wheels [29]. The wheel generates one excitation when it rolls a circle, which is then transmitted to the ABA. The consistent rotation of the wheel causes a periodic excitation in the ABA, which manifests as the dominant frequency f_z [20]. Consequently, the rotational frequency of the wheel corresponds to the excitation frequency produced by the wheel rotation, which is equivalent to the dominant frequency f_z. Therefore, Assumption (3) is valid.

Algorithm 1 Sensor Fusion Based on Kalman Filter

Input: vertical ABA sample set $V = \{V_i\}_{i=1}^{l}$, longitudinal ABA sample set $L = \{L_i\}_{i=1}^{l}$, the parameter R, Q, and P.
1: **for** $k = 1 \ldots l$ **do**
2: $P = P + Q$
3: $K = P/(P + Q)$
4: $F_k = L_k + K * (V_k - L_k)$
5: $P = (1-k)*P$
6: **end for**
Output: $F = \{F_k\}_{k=1}^{l}$: fusion data.

B. Data Fusion and Feature Extraction

In this module, our objective is to incorporate the obtained domain knowledge into feature design and extraction processes. A Kalman filter-based data fusion method was designed to combine the advantages of ABA signals from different directions. Subsequently, the knowledge-informed feature is extracted from the fused ABA data.

Vertical and longitudinal ABA have distinct advantages in predicting wheel wear. Specifically, the ABA in the longitudinal direction signifies that the dominant frequency is prompted by the wheel perimeter, which is closely correlated with wheel tread wear. However, the literature [28] reports that the longitudinal ABA can be distorted by additional wheel defects, namely wheel flats and rail squats, undermining the accuracy and reliability of wear predictions. Conversely, wheel tread wear occurs in the radial direction and is acquired by radial calculations. As a result, the vertical ABA offers more pronounced physical significance in this context than the longitudinal ABA. However, the vertical ABA is full of noise interference, which affects effective feature extraction.

In contrast, according to our analysis and conclusions drawn from [20] and [28], the lateral ABA exhibits more noise compared to the longitudinal ABA in terms of the dominant frequency and lacks the physical significance associated with the vertical ABA. Consequently, lateral ABA does not demonstrate a distinct advantage over vertical and longitudinal ABA.

Based on the preceding analysis, a sensor data fusion approach is designed to leverage the advantages of vertical and longitudinal ABA. Inspired by the Kalman filter's advantage for time-series fusion in real-time fusion, robustness to noise, and low computational burden [30], a Kalman filter-based sensor fusion method is proposed to fuse vertical and longitudinal ABA data. The fundamental concept behind the fusion algorithm is to employ longitudinal ABA data as a template to denoise the vertical ABA data in the time domain. This ensures that the modified vertical ABA data exhibit a dominant frequency associated with the wheel's perimeter, which is essential for subsequent feature extraction. The procedure of the fusion algorithm is detailed in Algorithm 1, with the initialization parameters R, Q, and P.

After acquiring the modified vertical ABA data, a domain knowledge-based feature design is investigated to extract the interpretable feature. The dominant frequency associated with the wheel perimeter is extracted from the modified vertical ABA using the FFT and the band filter method. Fig. 8 illustrates the extraction process of the dominant frequency band and the feature. The feature design in this study follows the following domain knowledge. As the wheel undergoes tread wear degradation and its radius decreases, the dominant frequency associated with the wheel's perimeter correspondingly increases, as indicated by (2). Consequently, we utilize the wheel perimeter-related dominant frequency as the feature to map wheel tread wear. The abscissa, namely position, corresponding to the largest peak within the specified area on the frequency spectrum, identifies the dominant frequency associated with train components [20]. To measure the position of the peak, the findpeak algorithm [31], [32] is employed, which is based on the curve's localized nature. It utilizes a Gaussian distribution and least-squares methods for curve fitting to accurately determine the peak's amplitude.

C. Regression Modeling

In this module, a support vector regression (SVR) model [33] is employed to predict the wheel tread wear using the feature extracted from the wheel perimeter-related dominant frequency. In real-world engineering scenarios, challenges often arise because of limited data samples and nonlinear relationships between the features and predicted values. The rationale for opting for SVR is its proficiency in addressing these challenges by leveraging the principles of support vectors and kernel functions. Among various advanced regression models, SVR is consistently recognized for its superior performance and robustness [34]. The core concept of SVR involves mapping the input vector from a primal space to a higher dimensional feature space using a nonlinear transformation.

In this study, each input vector is $x_i = [\text{frequency}_i]$, which is the wheel perimeter-related dominant frequency. Besides, each output vector $y_i = [\text{wear}_i]$ denotes the corresponding wheel tread wear. For the sample dataset $\{(x_i, y_i)\}_i^n$, linear regression is performed within the feature space

$$f(x_i) = \omega \cdot \phi(x_i) + b \tag{4}$$

where ω is the weight vectors, b is a set of biases, and $\phi(x)$ is a nonlinear mapping function.

Vapnik [35] proposed the ε-insensitive loss function based on the support vector machine to improve the model's generalization ability. The form of the ε-insensitive function is as follows:

$$L_\varepsilon(f(x_i) - y_i) = \begin{cases} 0, & |f(x_i) - y_i| \le \varepsilon \\ |f(x_i) - y_i| - \varepsilon, & |f(x_i) - y_i| > \varepsilon \end{cases} \tag{5}$$

where ε is the insensitivity loss factor (the maximum error allowed). Parameters ω and b of the SVR are formulated as the convex quadratic programming problem. The calculation formula is as follows:

$$\min_{\omega,b} L_p = \frac{1}{2}\sum_{j=1}^{Q}\left\|\omega^j\right\|^2 + C\sum_{i=1}^{n} L_\omega(f(x_i), y_i) \tag{6}$$

where C denotes the penalty factor. As the degree of slack is different on both sides of the spacer band, the slack variable $\{\xi_i\}_{i=1}^n$ and $\{\xi_{i_i}^*\}_{i=1}^n$ is introduced, and the following formula is obtained:

$$\min_{\omega,b,\xi_i,\xi_i^*} R(\omega, b, \xi) = \frac{1}{2}\sum_{j=1}^{Q}\left\|\omega^j\right\|^2 + C\sum_{i=1}^{n}\left(\xi_i + \xi_i^*\right). \tag{7}$$

Equation (7) can be converted into a dual problem

$$\begin{aligned}\max_{\alpha_i^*,\alpha_i} R\left(\alpha_i^*, \alpha_i\right) = &-\frac{1}{2}\sum_{i,j}^{n}\left(\alpha_i^* - \alpha_i\right)\left(\alpha_j^* - \alpha_j\right)\phi(x_i)\phi\left(x_j\right) \\ &- \sum_{i}^{n}\alpha_i(y_i + \varepsilon) + \sum_{i}^{n}\alpha_i^*(y_i - \varepsilon)\end{aligned} \tag{8}$$

where α_i and α_i^* are Lagrange multipliers. Mercer's theorem can solve the convex quadratic programming problem. The SVR function is obtained as follows:

$$\begin{aligned} f(x) &= \omega \cdot \phi(x) + b \\ &= \sum_{i}^{n}\left(\alpha_i - \alpha_i^*\right)\Phi(x_i)\Phi(x) + b \\ &= \sum_{i=1}^{N}\left(\alpha_i - \alpha_i^*\right)k(x_i x) + b \end{aligned} \tag{9}$$

where $k(x_i, x)$ is the kernel function.

IV. Experiments and Evaluation

A. Experimental Setup

The methodology is assessed using real-field multisource signal data involving the ABA, speed, and wheel wear, as described in Section II. This study focuses on the data gathered from Sensor 1 in Car 7 (C7) and Sensor 7 in Car 8 (C8), both in the axle box. The ABA data are selected because

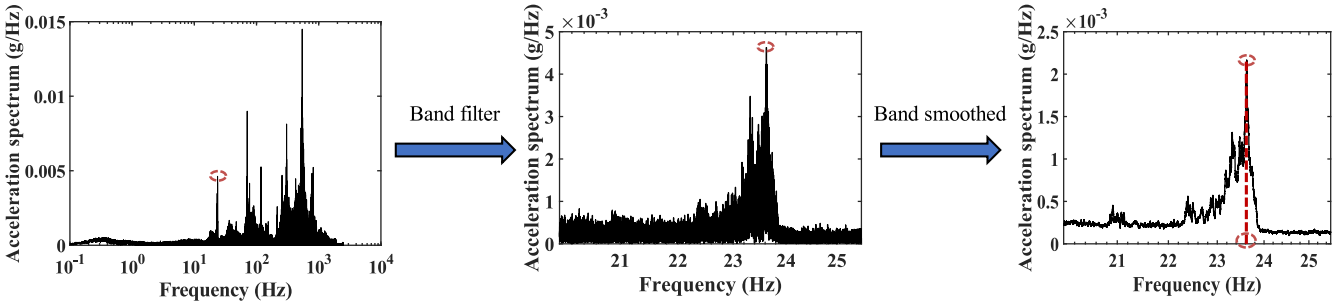

Fig. 8. Processing of the dominant frequency band and feature extraction.

of their proximity to the wheel, thereby providing a more precise mapping of the vibrational characteristics associated with the wheel. While C7 is a trailer car, C8 operates as a motor car, suggesting a distinct noisy environment for each. Specifically, C8 exhibits a heightened level of noise interference compared with C7.

To streamline subsequent experiments, we conduct comprehensive preprocessing of the field data, including data cleaning, normalization, and augmentation. As the data pertain to onsite vibrations between HSR wheels and tracks, certain complexities and anomalies arise because of factors such as track irregularities. In constructing the dataset, samples that exhibited abnormalities owing to interference factors were excluded to preserve the integrity of the correlation analysis between the extracted feature and wear. To ensure uniformity of scale and bolster the stability of the model, z-score normalization is applied to the ABA data. We employed a sliding-segmentation-based data augmentation method to fulfill the model training sample size requirements [19]. Fig. 9 illustrates the data augmentation procedure. Specifically, sliding window operations are performed on the ABA data during periods of stable speed with a window duration of 5 s. Given the uniform speed and identical test train used on both the GZ and SH lines, we have consolidated the data for a more cohesive analysis. Consequently, our study comprises four distinct datasets: Datasets 1 and 2 are associated with wheels monitored by sensors 1 and 7 on the CH line, respectively, whereas Datasets 3 and 4 pertain to wheels monitored using the same sensors on the combined GZ and SH lines. The datasets were each expanded to include 4300 samples, maintaining a training-to-test set distribution at the ratio of 4:1. Owing to hardware limitations, wheel wear predictions were conducted offline.

The models used in this study were executed on an offline workstation powered by an Intel i7-8700 CPU and an NVIDIA RTX 2080 GPU. We utilized Python 3.6, with the Keras framework for the ML-based approach, and MATLAB 2021 b for data processing. The model performance was assessed using mean absolute percentage error (MAPE), root mean square error (RMSE), and R^2 as evaluation metrics, addressing various facets of the analysis. In the training phase of our SVR models, we utilized the Gaussian radial basis function (RBF) kernel, which is defined as $k(m,n) = \exp(-\|m_i - n_j\|^2/2\sigma^2)$, where σ represents the kernel parameter. The model's performance is contingent on the fine-tuning of three hyperparameters: the kernel parameter σ, the regularization parameter C, and the epsilon-insensitive loss parameter ε. To identify the optimal values for these parameters, we used a fivefold cross-validation strategy within designated parameter ranges. The optimal parameter set is then chosen based on its ability to minimize the RMSE.

B. Case Study in Operation Datasets

1) Effectiveness of the Proposed Fusion Method: In this section, we assess the performance of the designed Kalman filter-based data fusion method. Specially, the fusion method is applied to the vertical ABA data using the longitudinal ABA data as a template for correction.

The verification process comprises two stages. First, we implement FFT and STFT on the corrected vibration signal to observe whether the noise is reduced and whether the wheel perimeter-induced dominant frequency appears. Subsequently, we extract the frequency vector from the dominant frequency band and compare it with the speed vector for correlation assessment. The Pearson correlation coefficient is used as the evaluation metric. To evaluate the corrective efficacy of the vertical ABA signal, we employ raw ABA data instead of the augmented dataset for the analysis because the validation approach does not involve model construction. Fig. 10 illustrates the spectrum and spectrogram of the original and corrected vertical ABA signals using vibration measurements from C8 during one trip as a representative sample.

Fig. 10(a) presents the original vertical vibration data in the frequency domain from FFT. Fig. 10(c) illustrates the same data in the time–frequency domain after STFT. Although two peak regions are evident in the spectrum, the pervasive noise interference in the time–frequency domain masks the dominant frequency. Fig. 10(b) and (d) shows the frequency and time–frequency domain representations of the corrected vertical ABA signal following FFT and STFT, respectively. Significant noise reduction can be observed, underscoring the effectiveness of the designed data fusion method. Fig. 11 shows the average Pearson coefficients for the three lines. Notably, the coefficients for C7 and C8 exceed 0.85, suggesting a strong linear correlation and proving the effectiveness of the proposed fusion method. The higher coefficient of C7 compared with C8 can be ascribed to the distinct roles of the respective vehicles: C7 serves as a trailer, whereas C8

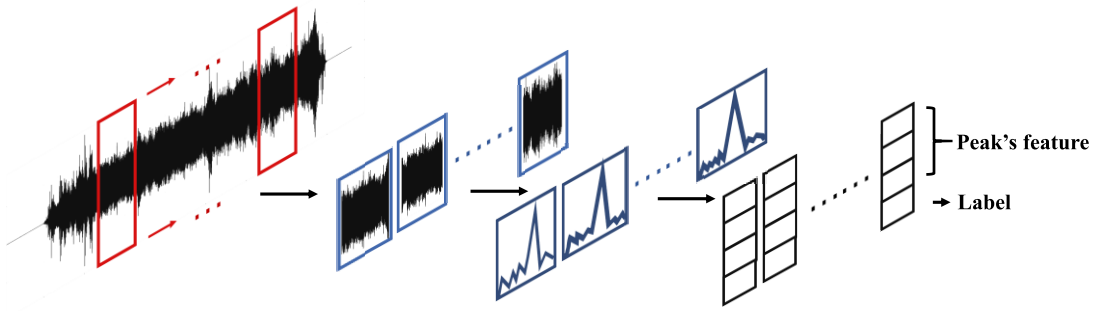

Fig. 9. Process of data augmentation with sliding window operations.

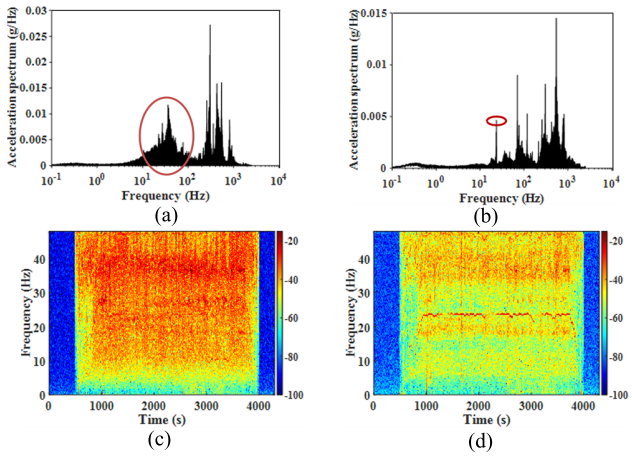

Fig. 10. Diagram of the fusion effect for the designed fusion algorithm. (a) Spectrum in original vertical vibration data. (b) Spectrum in corrected vertical vibration data. (c) Spectrogram in original vertical vibration data. (d) Spectrogram in corrected vertical vibration data.

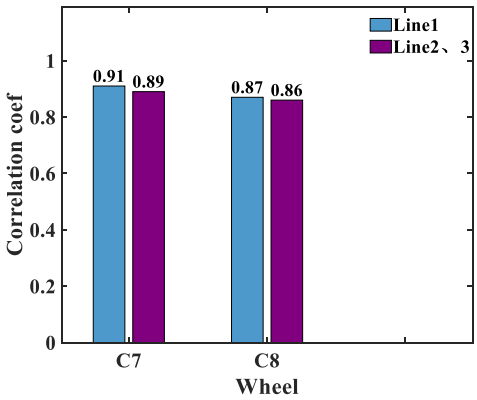

Fig. 11. Correlation comparison results.

functions as a power car, with the latter intrinsically exhibiting more noise.

2) Effectiveness of the Proposed Feature: In this section, we compare the proposed feature derived from the corrected vertical ABA data to its counterpart obtained from the original ABA data across three directions. The position of the largest peak within the first peak region of the original vertical ABA data is identified as the feature. For longitudinal and lateral ABA data, the dominant frequency induced by the wheel perimeter is selected as the feature. The feature is extracted using a bandpass filter and the findpeak algorithm. The models for the corrected vertical ABA, vertical ABA, longitudinal ABA, and lateral ABA are denoted as Model-F, Model-V, Model-LO, and Model-LA, respectively. To ensure a fair evaluation, SVR is uniformly adopted for modeling.

Table II lists the experimental results for the four datasets. Notably, when comparing the performance of the original vertical, longitudinal, and lateral vibration data, the accuracy of Model-LO distinctly outperforms the other two models. This demonstrates that the longitudinal ABA experiences less noise interference and contains more valuable information. This observation is consistent with the domain knowledge discussed in Section III. Conversely, the performance of Model-V is noticeably inferior owing to noise interference. Additionally, it is evident that Model-F's accuracy has substantially improved, surpassing those of Model-LO, Model-LA, and Model-V. For instance, in the experiment conducted with C7 in Line 1, Model-F achieved the MAPE of 0.0752; whereas Model-LO, Model-LA, and Model-V registered MAPE values of 0.0868, 0.1204, and 0.3220, respectively. These results underscore the effectiveness of the proposed approach.

3) Compared With Manual Feature-Based Approaches: The proposed wheel tread wear prediction method is compared with the other manual feature-based methods in the existing literature. The methodology focuses on manual features and incorporates elements from the time, frequency, and time–frequency domains, denoted by Model 1, Model 2, and Model 3. An in-depth description of the comparative methods is as follows.

1) *Model 1:* The time domain manual features, as outlined in [36], including waveform length (WL), root mean square (RMS), and kurtosis (KURT).
2) *Model 2:* The frequency domain manual features, as outlined in [37], comprise the grand mean, variance, and third-order cumulant.
3) *Model 3:* The time-frequency domain manual features, as delineated in the literature [15], focus on the energy of the dominant frequency dependent on the wheel radius.

To ensure consistent evaluation, SVR is uniformly applied during the modeling stage. Table III presents the experimental results obtained for the four datasets. Notably, the performance of the proposed method surpasses that of Models 1, 2, and 3. For instance, in the experiment conducted on C7 in Line 1, it can be observed that Model-F obtained the MAPEs of

TABLE II
PERFORMANCES OF MODEL-F, MODEL-V, MODEL-LO, AND MODEL-LA

		Line 1				Line 2 and 3			
		Model-V	**Model-LO**	**Model-LA**	**Model-F**	**Model-V**	**Model-LO**	**Model-LA**	**Model-F**
Car 7	**MAPE**	0.3220	0.0868	0.1204	**0.0752**	0.6241	0.1078	0.1340	**0.0831**
	RMSE	0.0416	0.0133	0.0153	**0.0104**	0.1596	0.0426	0.0554	**0.0308**
	R^2	0.0677	0.9045	0.8745	**0.9414**	0.1038	0.9360	0.8919	**0.9666**
Car 8	**MAPE**	0.4007	0.1262	0.1520	**0.1182**	0.6895	0.1173	0.1412	**0.0992**
	RMSE	0.0146	0.0061	0.0067	**0.0054**	0.1758	0.0433	0.0448	**0.0428**
	R^2	0.0003	0.8872	0.8598	**0.9338**	0.0042	0.9396	0.9353	**0.9410**

TABLE III
PERFORMANCES OF MODEL-F, MODEL 1, MODEL 2, AND MODEL 3

		Line 1				Line 2 and 3			
		Model 1	**Model 2**	**Model 3**	**Model-F**	**Model 1**	**Model 2**	**Model 3**	**Model-F**
Car 7	**MAPE**	0.1602	0.1241	0.0917	**0.0752**	0.1785	0.1462	0.1140	**0.0831**
	RMSE	0.0223	0.0169	0.0117	**0.0104**	0.0659	0.0455	0.0427	**0.0308**
	R^2	0.7310	0.8455	0.9260	**0.9414**	0.8473	0.9272	0.9359	**0.9666**
Car 8	**MAPE**	0.2524	0.1850	0.1578	**0.1182**	0.2572	0.1471	0.1275	**0.0992**
	RMSE	0.0951	0.0094	0.0089	**0.0054**	0.1039	0.0531	0.0441	**0.0428**
	R^2	0.7089	0.9218	0.9296	**0.9338**	0.6520	0.9092	0.9374	**0.9410**

0.0752, while Models 1, 2, and 3 obtained the MAPEs of 0.1602, 0.1241, and 0.0917, respectively. These results highlight the effectiveness of the proposed method. Notably, in Tables II and III, apart from the proposed method, some indicators show that C8 outperforms C7 under the same conditions. This variation arises because real-world data typically include varying degrees of noise, and different methods have different anti-noise capabilities. For the difference in RMSE, C8's wheel is newer with an RMSE in the lower range on Line 1, whereas C7's wheel, which has been worn longer, exhibits an RMSE in the higher range. On Lines 2 and 3, the RMSE values for C8 exceed those of C7, indicating that the motor car's wheel is more susceptible to wear.

4) Compared With Deep Learning-Based Approaches: In this section, the proposed wheel tread wear prediction method is compared with the deep learning-based approach in the existing literature. The methodology focuses on automatic features within the time domain under 1-D vibration data representation, denoted by ResNet18, Xception, and LGF-Trans. An in-depth description of the comparative method is as follows.

1) *ResNet18:* 1-D residual modules, of which the total number of convolutional layers is 18, as described in the literature [36].
2) *Xception:* 1D-Xception is a CNN architecture composed of deep separable convolution. We modified it into a 1-D version while following its original structure, as described in the literature [36].
3) *LGF-Trans:* LGF-Trans comprises eight LTA-Networks and eight transformer encoder layers, with parameters k and H both set to 8, and T set to 3072. Following the transformer layers, two fully connected layers consolidate the outputs to predict wheel tread wear values, as detailed in the literature [36].

The tread wear prediction results of these models are shown in Table IV. Notably, the proposed method outperforms ResNet18, Xception, and LGF-Trans. For instance, in the experiment conducted on Car7 in Line 1, it can be observed that Model-F obtained MAPE in 0.0752, while ResNet18, Xception, and LGF-Trans obtained MAPE in 0.1141, 0.1358, and 0.0821, respectively. These results highlight the efficacy of our proposed method. Additionally, the performance of the comparison models is influenced by noise interference, which may occasionally lead to C8 outperforming C7 in terms of some indicators.

5) Anti-Interference Performance Analysis: An analysis of sensitivity is conducted to evaluate the anti-interference ability of the proposed method when faced with different levels of noise. As reported in the literature [38], Gaussian noise with different specific signal-to-noise ratios (SNR) is added to the test dataset used in experiments 3) and 4). To intuitively observe the changes in performance, we adopt MAPE as the evaluation metric. Fig. 12 shows the experiment results. It is evident that the proposed method delivers relatively stable outcomes, as demonstrated by the MAPE fluctuation being less than 5%.

TABLE IV
PERFORMANCES OF MODEL-F, RESNET18, XCEPTION, AND LGF-TRANS

		Line 1				Line 2 and 3			
		ResNet18	Xception	LGF-Trans	Model-F	ResNet18	Xception	LGF-Trans	Model-F
Car 7	MAPE	0.1141	0.1358	0.0821	**0.0752**	0.1294	0.1438	0.0917	**0.0831**
	RMSE	0.0171	0.0196	0.0128	**0.0104**	0.0581	0.0660	0.0499	**0.0308**
	R^2	0.8419	0.7937	0.9119	**0.9414**	0.9070	0.8898	0.9334	**0.9666**
Car 8	MAPE	0.1615	0.1509	0.1275	**0.1182**	0.1706	0.1476	0.1127	**0.0992**
	RMSE	0.0103	0.0088	0.0058	**0.0054**	0.0836	0.0823	0.0604	**0.0428**
	R^2	0.9050	0.9298	0.9309	**0.9338**	0.8261	0.7946	0.8857	**0.9410**

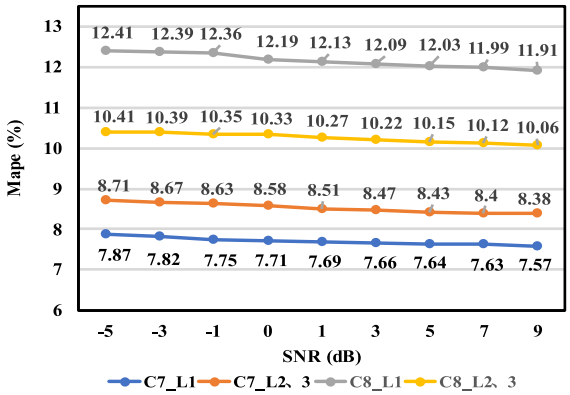

Fig. 12. Performance of the proposed method across various noise levels.

In summary, the following conclusions can be drawn: 1) the designed Kalman-based fusion method proves effective in denoising and correcting the vertical ABA; 2) the quality of the feature, derived from our domain knowledge, is commendable; and 3) the knowledge-based feature significantly enhances the prediction performance, even in the presence of high-intensity noise.

V. CONCLUSION

In this study, we developed a domain-knowledge-guided data-driven method to predict wheel tread wear. The developed method includes three modules: 1) spectral analysis and knowledge conclusion; 2) data fusion and feature extraction; and 3) regression modeling. First, the ABA data are investigated using spectral analysis, and the domain knowledge associated with wheel tread wear is concluded. Subsequently, data fusion is performed to denoise and modify the vertical ABA signals and feature extraction. Finally, a regression model is built to map the relationship between the wheel tread wear and the extracted features. In the comparative experiments against methods utilizing manually extracted features, our proposed method demonstrated average reductions in MAPE by 55.27%, 37.81%, and 23.10% relative to time domain features, frequency domain features, and time-frequency domain features, respectively. In the experiments comparing deep-learning approaches that leverage automatic feature extraction, our method achieved average reductions in MAPE of 34.63%, 35.32%, and 9.26% when compared with ResNet18, Xception, and LGF-Trans, respectively. By integrating mechanical insights with data-driven methods, our approach negates the need for intricate physical modeling and remains interpretable with knowledge-based features.

The method proposed in this study is specifically designed for employing vibration acceleration modeling during the steady-state phase; hence, it has limitations when applied to scenarios with nonstationary velocities. In future work, our research will delve deeper into the domain knowledge associated with deep learning methods. This will follow the precedent set in the literature [39], which first explored and explained the confidence and uncertainty in the fault diagnosis results of deep learning methods, making some progress on interpretable intelligent fault diagnosis. In addition, we aim to enhance our prediction methodologies to accommodate a range of operational conditions, specifically those involving dynamic speed changes.

REFERENCES

[1] W. Luo. *China's High-Speed Rail Extends Up to 45,000 Km, China Daily*. Accessed: Jan. 9, 2024. [Online]. Available: https://www.chinadaily.com.cn/a/202401/09/WS659d49b1a3105f21a507b691.html
[2] R. Enblom, "Deterioration mechanisms in the wheel–rail interface with focus on wear prediction: A literature review," *Vehicle Syst. Dyn.*, vol. 47, no. 6, pp. 661–700, Jun. 2009.
[3] T. Jendel, "Prediction of wheel profile wear—Comparisons with field measurements," *Wear*, vol. 253, nos. 1–2, pp. 89–99, Jul. 2002.
[4] J. Lin, H. Shao, X. Zhou, B. Cai, and B. Liu, "Generalized MAML for few-shot cross-domain fault diagnosis of bearing driven by heterogeneous signals," *Expert Syst. Appl.*, vol. 230, Nov. 2023, Art. no. 120696.
[5] W. Zhang, Z. Shen, and J. Zeng, "Study on dynamics of coupled systems in high-speed trains," *Vehicle Syst. Dyn.*, vol. 51, no. 7, pp. 966–1016, Jul. 2013.
[6] J. J. Kalker, "Wheel-rail rolling contact theory," *Wear*, vol. 144, nos. 1–2, pp. 243–261, Apr. 1991.
[7] J. Pombo, J. Ambrósio, and M. Silva, "A new wheel-rail contact model for railway dynamics," *Vehicle Syst. Dyn.*, vol. 45, no. 2, pp. 165–189, Feb. 2007.
[8] A. Chudzikiewicz, "Modelling of wheel and rail wear," *Arch. Transp.*, vol. 13, no. 2, pp. 5–24, 2001.
[9] I. Zobory, "Prediction of wheel/rail profile wear," *Vehicle Syst. Dyn.*, vol. 28, nos. 2–3, pp. 221–259, Aug. 1997.

[10] A. Szabó and I. Zobory, "Wheel-profile wear simulation in case of operation on a specified railway network," *Eur. Railway Rev.*, vol. 4, pp. 86–89, Jan. 2003.
[11] J. F. Archard, "Contact and rubbing of flat surfaces," *J. Appl. Phys.*, vol. 24, no. 8, pp. 981–988, Aug. 1953.
[12] C. R. Á. da Silva and G. Pintaude, "Uncertainty analysis on the wear coefficient of Archard model," *Tribol. Int.*, vol. 41, no. 6, pp. 473–481, Jun. 2008.
[13] Y. Li, Z. Ren, R. Enblom, S. Stichel, and G. Li, "Wheel wear prediction on a high-speed train in China," *Vehicle Syst. Dyn.*, vol. 58, no. 12, pp. 1839–1858, Dec. 2020.
[14] B. Huang, M. E, Z. Jiang, and Q. Li, "Prognosis of wheel tread degradation status based on PCA-NARX neural network," in *Proc. Global Rel. Prognostics Health Manage. (PHM-Shanghai)*, Oct. 2020, pp. 1–6.
[15] P. Han and W.-H. Zhang, "A new binary wheel wear prediction model based on statistical method and the demonstration," *Wear*, vols. 324–325, pp. 90–99, Feb. 2015.
[16] P. Xu et al., "Condition monitoring of wheel wear for high-speed trains: A data-driven approach," in *Proc. IEEE Int. Conf. Prognostics Health Manage. (ICPHM)*, Jun. 2018, pp. 1–8.
[17] L. Chen, N. Qin, X. Dai, and D. Huang, "Fault diagnosis of high-speed train bogie based on capsule network," *IEEE Trans. Instrum. Meas.*, vol. 69, no. 9, pp. 6203–6211, Sep. 2020.
[18] D. Huang, S. Li, N. Qin, and Y. Zhang, "Fault diagnosis of high-speed train bogie based on the improved-CEEMDAN and 1-D CNN algorithms," *IEEE Trans. Instrum. Meas.*, vol. 70, pp. 1–11, 2021.
[19] H. Wang, T. Men, and Y.-F. Li, "Transformer for high-speed train wheel wear prediction with multiplex local–global temporal fusion," *IEEE Trans. Instrum. Meas.*, vol. 71, pp. 1–12, 2022.
[20] W. Zhai, P. Liu, J. Lin, and K. Wang, "Experimental investigation on vibration behaviour of a CRH train at speed of 350 km/h," *Int. J. Rail Transp.*, vol. 3, no. 1, pp. 1–16, Jan. 2015.
[21] M. Maglio, T. Vernersson, J. C. O. Nielsen, A. Ekberg, and E. Kabo, "Influence of railway wheel tread damage on wheel–rail impact loads and the durability of wheelsets," *Railway Eng. Sci.*, early access, Aug. 16, 2023, doi: 10.1007/s40534-023-00316-2.
[22] X. Wang, J. Zhang, and J. Zuo, "Wheel tread wear prediction of high-speed railway train," *Tribol. Lett.*, vol. 70, no. 2, p. 62, Jun. 2022.
[23] S. Li, H. Fang, and B. Shi, "Remaining useful life estimation of lithium-ion battery based on interacting multiple model particle filter and support vector regression," *Rel. Eng. Syst. Saf.*, vol. 210, Jun. 2021, Art. no. 107542.
[24] M. Molodova, Z. Li, and R. Dollevoet, "Axle box acceleration: Measurement and simulation for detection of short track defects," *Wear*, vol. 271, nos. 1–2, pp. 349–356, May 2011.
[25] B. Yang, "A study of inverse short-time Fourier transform," in *Proc. IEEE Int. Conf. Acoust., Speech Signal Process.*, Mar. 2008, pp. 3541–3544.
[26] H. V. Poor and S. M. Zabin, "Efficient estimation of class a noise parameters via the EM algorithm," *IEEE Trans. Inf. Theory*, vol. 37, no. 1, pp. 60–72, Jan. 1991.
[27] S. Luo, X. Li, and G. Bi, "Short-time lv transform and its application for non-linear FM signal detection," *J. Syst. Eng. Electron.*, vol. 26, no. 6, pp. 1159–1168, Dec. 2015.
[28] Z. Li, M. Molodova, A. Nú nez, and R. Dollevoet, "Improvements in axle box acceleration measurements for the detection of light squats in railway infrastructure," *IEEE Trans. Ind. Electron.*, vol. 62, no. 7, pp. 4385–4397, Jul. 2015.
[29] Q. Sun, C. Chen, A. H. Kemp, and P. Brooks, "An on-board detection framework for polygon wear of railway wheel based on vibration acceleration of axle-box," *Mech. Syst. Signal Process.*, vol. 153, May 2021, Art. no. 107540.
[30] Y. Zhang, M. Li, Y. Zhang, Z. Hu, Q. Sun, and B. Lu, "An enhanced adaptive unscented Kalman filter for vehicle state estimation," *IEEE Trans. Instrum. Meas.*, vol. 71, pp. 1–12, 2022.
[31] T. C. O'Haver. *Peak Finding and Measurement*. Accessed: Dec. 9, 2018. [Online]. Available: https://terpconnect.umd.edu/~toh/spectrum/PeakFindgandMeasurement.htm
[32] N. Hong et al., "High-speed rail suspension system health monitoring using multi-location vibration data," *IEEE Trans. Intell. Transp. Syst.*, vol. 21, no. 7, pp. 2943–2955, Jul. 2020.
[33] H. Drucker, C. J. Burges, L. Kaufman, A. J. Smola, and V. Vapnik, "Support vector regression machines," in *Proc. Int. Conf. Neural Inf. Process. Syst.*, 1997, pp. 155–161.
[34] C. Yang, P. An, and L. Shen, "Blind image quality measurement via data-driven transform-based feature enhancement," *IEEE Trans. Instrum. Meas.*, vol. 71, pp. 1–12, 2022.
[35] V. N. Vapnik, "An overview of statistical learning theory," *IEEE Trans. Neural Netw.*, vol. 10, no. 5, pp. 988–999, Sep. 1999.
[36] B. R. Nayana and P. Geethanjali, "Analysis of statistical time-domain features effectiveness in identification of bearing faults from vibration signal," *IEEE Sensors J.*, vol. 17, no. 17, pp. 5618–5625, Sep. 2017.
[37] C.-G. Zhou, Y.-C. Gu, C.-H. Nie, Y. Ou, and H.-T. Feng, "Detecting preload degradation of a ball screw feed system using high-frequency reconstruction and support vector machine," *J. Vibrat. Control*, vol. 29, nos. 19–20, pp. 4514–4525, Oct. 2023.
[38] Y. Xiao, H. Shao, J. Wang, S. Yan, and B. Liu, "Bayesian variational transformer: A generalizable model for rotating machinery fault diagnosis," *Mech. Syst. Signal Process.*, vol. 207, Jan. 2024, Art. no. 110936.
[39] Y. Xiao, H. Shao, M. Feng, T. Han, J. Wan, and B. Liu, "Towards trustworthy rotating machinery fault diagnosis via attention uncertainty in transformer," *J. Manuf. Syst.*, vol. 70, pp. 186–201, Oct. 2023.

Chen Chen (Student Member, IEEE) is currently pursuing the joint Ph.D. degree from Tongji University, Shanghai, China, and City University of Hong Kong, Hong Kong, China.

His research interests include developing analytical approaches for the intelligent operation and maintenance of rail transportation systems.

Feng Zhu received the dual B.S. degree in mechanical engineering from Chongqing University, Chongqing, China, and the University of Cincinnati, Cincinnati, OH, USA, in 2018, and the M.S. degree in mechanical engineering from the University of Cincinnati, in 2020. He is currently pursuing the Ph.D. degree in industrial engineering with the Department of Systems Engineering, City University of Hong Kong, Hong Kong.

His current research interests include prognostic and health management, data mining, and machine learning.

Zhongwei Xu received the Ph.D. degree from Tongji University, Shanghai, China, in 2005.

Since 2009, he has been a Professor with Tongji University. He is currently the Chief of the Interlock Station of Inspection and the Test Center of the China Academy of Railway Sciences, Shanghai. His research interests include automated debugging, testing, and formal verification.

Qinglin Xie (Graduate Student Member, IEEE) received the B.S. degree in engineering mechanics and the M.S. degree in vehicle engineering from Southwest Jiaotong University, Chengdu, China, in 2018 and 2021, respectively, where he is currently pursuing the Ph.D. degree in vehicle operation engineering with the State Key Laboratory of Rail Transit Vehicle System.

His research interests include SHM data mining, rail transit digital platform construction, and intelligent operation and maintenance.

Siu Ming Lo received the Ph.D. degree in architecture from The University of Hong Kong, Hong Kong.

He is currently a Professor with the Department of Architecture and Civil Engineering, City University of Hong Kong, Hong Kong. His current research interests include urban and land use planning, spatial planning for pedestrian movement and evacuation modeling, and building development.

Kwok Leung Tsui received the Ph.D. degree in statistics from the University of Wisconsin–Madison, Madison, WI, USA, in 1986.

He is currently a Professor with the Grado Department of Industrial and Systems Engineering, Virginia Polytechnic and State University, Blacksburg, VA, USA. His current research interests include data science and data analytics, surveillance in healthcare and public health, personalized health monitoring, prognostics and systems health management, and process control and monitoring.

Dr. Tsui is a Fellow of INFORMS, the American Statistical Association, American Society for Quality, the International Society of Engineering Asset Management, and the Hong Kong Institution of Engineers, an elected Council Member of the International Statistical Institute, and a U.S. Representative to the ISO Technical Committee on Statistical Methods.

Lishuai Li (Senior Member, IEEE) received the Ph.D. and M.Sc. degrees in air transportation systems from the Department of Aeronautics and Astronautics at Massachusetts Institute of Technology (MIT), Cambridge, MA, USA, and B.Eng. degree in aircraft design and engineering from Fudan University, Shanghai, China.

She is an Associate Professor with the School of Data Science and Department of Mechanical Engineering at the City University of Hong Kong, Hong Kong. She was a consultant at McKinsey and Company with the Operations Practice in San Francisco. Her research interests include interdisciplinary field of intelligent transportation systems and data science.